

# Fiber Bragg gratings-based sensing for real-time needle tracking during MR-guided brachytherapy

Maxence Borot de Battisti<sup>a)</sup>

*Department of Radiotherapy, University Medical Center Utrecht, Heidelberglaan 100, Utrecht 3584 CX, The Netherlands*

Baudouin Denis de Senneville

*Imaging Division, University Medical Center Utrecht, Heidelberglaan 100, Utrecht 3584 CX, The Netherlands and IMB, UMR 5251 CNRS/University of Bordeaux, Talence 33400, France*

Metha Maenhout, Jan J. W. Lagendijk, and Marco van Vulpen

*Department of Radiotherapy, University Medical Center Utrecht, Heidelberglaan 100, Utrecht 3584 CX, The Netherlands*

Gilion Hautvast and Dirk Binnekamp

*Philips Group Innovation Biomedical Systems, Eindhoven 5656 AE, The Netherlands*

Marinus A. Moerland

*Department of Radiotherapy, University Medical Center Utrecht, Heidelberglaan 100, Utrecht 3584 CX, The Netherlands*

(Received 21 March 2016; revised 18 July 2016; accepted for publication 13 August 2016; published 6 September 2016; corrected 13 September 2016)

**Purpose:** The development of MR-guided high dose rate (HDR) brachytherapy is under investigation due to the excellent tumor and organs at risk visualization of MRI. However, MR-based localization of needles (including catheters or tubes) has inherently a low update rate and the required image interpretation can be hampered by signal voids arising from blood vessels or calcifications limiting the precision of the needle guidance and reconstruction. In this paper, a new needle tracking prototype is investigated using fiber Bragg gratings (FBG)-based sensing: this prototype involves a MR-compatible stylet composed of three optic fibers with nine sets of embedded FBG sensors each. This stylet can be inserted into brachytherapy needles and allows a fast measurement of the needle deflection. This study aims to assess the potential of FBG-based sensing for real-time needle (including catheter or tube) tracking during MR-guided intervention.

**Methods:** First, the MR compatibility of FBG-based sensing and its accuracy was evaluated. Different known needle deflections were measured using FBG-based sensing during simultaneous MR-imaging. Then, a needle tracking procedure using FBG-based sensing was proposed. This procedure involved a MR-based calibration of the FBG-based system performed prior to the interventional procedure. The needle tracking system was assessed in an experiment with a moving phantom during MR imaging. The FBG-based system was quantified by comparing the gold-standard shapes, the shape manually segmented on MRI and the FBG-based measurements.

**Results:** The evaluation of the MR compatibility of FBG-based sensing and its accuracy shows that the needle deflection could be measured with an accuracy of 0.27 mm on average. Besides, the FBG-based measurements were comparable to the uncertainty of MR-based measurements estimated at half the voxel size in the MR image. Finally, the mean(standard deviation) Euclidean distance between MR- and FBG-based needle position measurements was equal to 0.79 mm(0.37 mm). The update rate and latency of the FBG-based needle position measurement were 100 and 300 ms, respectively.

**Conclusions:** The FBG-based needle tracking procedure proposed in this paper is able to determine the position of the complete needle, under MR-imaging, with better accuracy and precision, higher update rate, and lower latency compared to current MR-based needle localization methods. This system would be eligible for MR-guided brachytherapy, in particular, for an improved needle guidance and reconstruction. © 2016 American Association of Physicists in Medicine. [<http://dx.doi.org/10.1118/1.4961743>]

Key words: needle tracking, real-time, MR-guided intervention, fiber Bragg grating, optic fiber

## 1. INTRODUCTION

HDR brachytherapy involves placement of needles (including catheters or tubes) into or close to the tumor, through

which a radioactive source (e.g., Ir-192) irradiates the tumor for certain times at different positions according to a calculated dose plan.<sup>1</sup> In usual clinical practice, a dose plan is made at the beginning of the brachytherapy procedure.<sup>2-4</sup>

This process involves selecting the appropriate needle positions in order to achieve an optimal dose distribution with a high irradiation dose to the tumor and the lowest possible dose to surrounding healthy tissues. However, two major events are likely to modify the preplanned dose distribution during the interventional process. First, needle positioning errors may occur: in the case of HDR prostate brachytherapy, Strassmann *et al.*<sup>5</sup> showed that the average needle positioning accuracy on prostate was  $2.7 \pm 0.7$  mm with manual template-guided insertion and  $1.8 \pm 0.6$  mm with robot-assisted positioning. Second, accidental shift (movement of patient), peristaltic change, bladder filling,<sup>6,7</sup> or internal movement of organs and tissue edema related to the trauma of the needle insertion<sup>8–10</sup> can cause anatomical modifications (and needle position deviations) during the intervention. Those events can lead to uncertainties and errors in the delivered dose to the planning target volume (PTV) and organs at risk (OARs).<sup>11</sup> To reduce those uncertainties, two methods are possible: (1) restraining at maximum the needle positioning errors and (2) dynamically updating the dose plan with feedback on the actual catheter locations as shown by Borot de Battisti *et al.*<sup>12</sup> For that, the real-time determination of the needle position (consisting of tracking the needle during insertion and reconstructing the needle after insertion) is warranted.

For an increasing number of brachytherapy applications, MRI is the imaging modality of choice due to excellent tumor and organs at risk (OARs) visualization.<sup>13–16</sup> de Oliveira *et al.*<sup>17</sup> proposed a needle tracking method using MRI in the case of endorectal biopsy device: it consists of applying a pulse sequence in order to follow a passive marker attached to the MR biopsy device holder. With this method, the position of the needle axis is automatically identified using a phase-only cross-correlation algorithm. The total duration of the tracking sequence is about 10 min. More recently, an active MR-tracking (MRTR) system was developed to provide accurate and rapid localization of interstitial brachytherapy catheters.<sup>18</sup> This system consists of integrating multiple microcoils into the metallic stylets that are used to advance the catheters into tissue. The catheter trajectory is reconstructed by pulling out the stylet from the catheter while the microcoils are tracked using a dedicated MR sequence. The mean 3D error of the catheter path was found to be  $1.5 \pm 0.5$  mm for an acquisition time of  $\sim 10$  s/catheter. In practice, the update rate of the needle position measurement in MRI may be too low and the latency too high for high-precision needle steering during the interventional procedure.

As an alternative to MR-based needle tracking, the needle shape can also be measured using a MR-compatible stylet with embedded fiber Bragg gratings (FBG) sensors. Park *et al.* and Henken *et al.*<sup>19,20</sup> were able to reconstruct the needle shape with high accuracy, but both only assessed in-plane needle deflection in free space. Roesthuis *et al.*<sup>21</sup> validated the accuracy of needle tip measurements using FBG sensors for out-of-plane (3D) deflections in both free space and a soft tissue simulant with a maximum out of plane error of 1.66 mm. Besides, Park *et al.* and Henken *et al.* both estimated needle curvature by measuring the curvature at two locations along the needle shaft (their stylets were composed

of three fibers with two sets of FBG sensors each). Roesthuis *et al.* used three fibers with four sets of FBG sensors each, which enabled to measure needle curvature at four different locations along the needle shaft. In this paper, an upgraded prototype is investigated: it includes an MR-compatible stylet involving three fibers with nine embedded sets of FBG sensors each. This FBG-based tracking system has potentially an improved accuracy and precision, higher update rate, and lower latency compared to MR-based needle tracking. Furthermore, the FBG-based sensing stylet is composed of MR-compatible materials which do not interfere with MR-imaging. However, the major issue of FBG-based sensing is that it only measures the deflection of the needle (i.e., the relative shape in the needle coordinate system). In order to assess the needle shape in the physical spatial coordinate system, the position and orientation of the stylet at, at least, one point of the stylet must be known.

This study aims to assess the potential of FBG-based sensing for real-time needle (including catheters or tubes) tracking during MR-guided intervention. The main contribution of this work is as follows:

- To evaluate the MR-compatibility and accuracy of the needle deflection measurement using FBG-based sensing.
- To propose an experimental protocol designed to assess needle tracking using FBG-based sensing. This protocol involves (1) the fixation in space of the stylet base and (2) a MR-based calibration which aims to determine the position and orientation of the stylet at the fixation point. This calibration is performed once and for all, prior to the measurement of the needle position. The authors underline that in practice, the proposed protocol is optional if the position and orientation of the stylet at one point are already known.
- To assess the FBG-based needle tracking procedure under MR-imaging in a phantom experiment.

Special attention will be paid to the accuracy, precision, update rate, and latency of the proposed needle tracking method.

## 2. METHODS

First, we describe the MR-compatible FBG-based sensing device (cf. Sec. 2.A). An inherent deficit of the FBG-based sensing is reported in this section: In order to assess the needle position in the physical spatial coordinate system, the position and orientation of the stylet at one or more stylet points are mandatory. To achieve this, we propose an experimental protocol which involves the fixation of the stylet base and a MR-based calibration performed prior to the measurement of the needle position (cf. Sec. 2.B). The experiments to evaluate the MR compatibility of the FBG-based sensing are described in Sec. 2.C.1: the accuracy of the needle deflection measurement is evaluated under on-line MRI. An experiment, which aims to assess the proposed FBG-based needle tracking procedure, is described in Sec. 2.C.2: this experiment involves the tracking of needles inserted in a moving phantom.

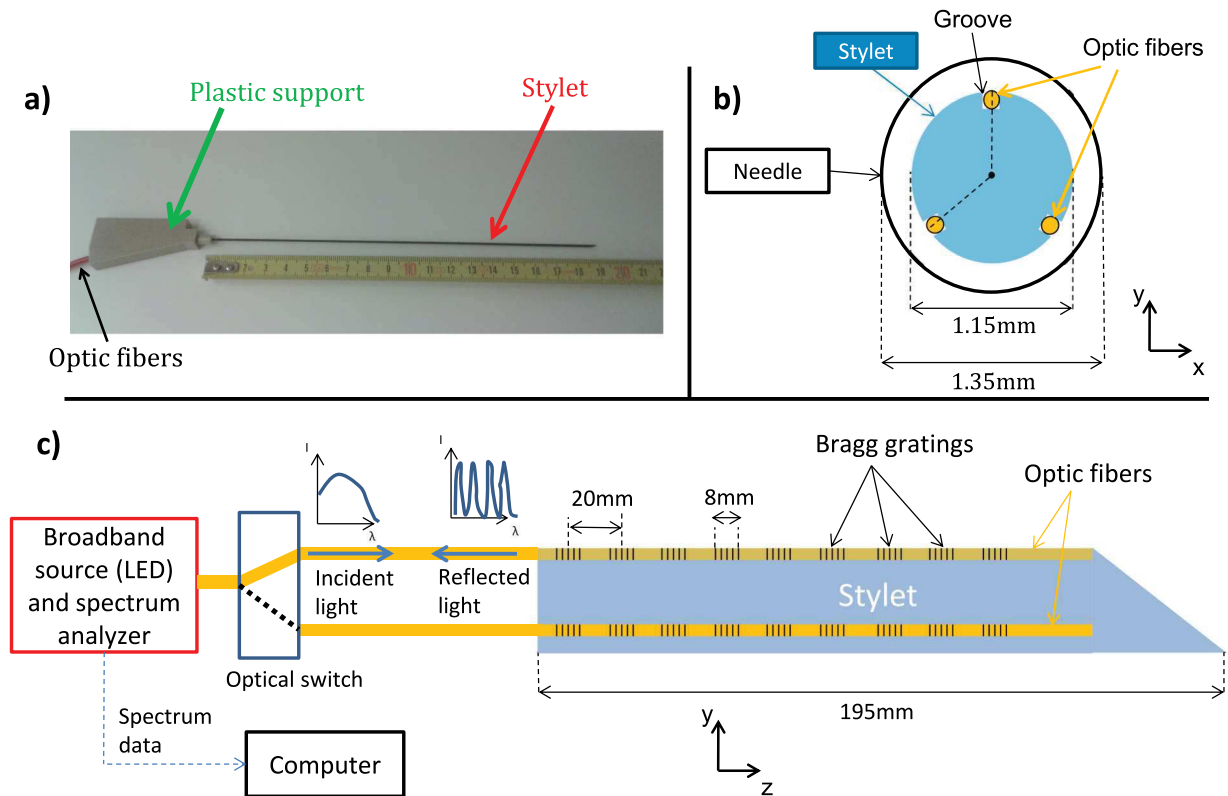


Fig. 1. (a) presents a picture of the FBG-based sensing stylet. (b) is a schematic of a transverse slice of the FBG-based sensing stylet inserted in the needle. (c) presents the longitudinal schematic of the stylet.

## 2.A. MR-compatible FBG-based sensing device

In the scope of this study, a FBG-based sensing prototype was used to determine the deflection of a brachytherapy needle in real-time. This FBG-based sensing prototype was composed of a MR-compatible stylet that can be inserted inside the lumen of the needle. The length of the stylet was  $195 \pm 1$  mm and the diameter  $1.15 \pm 0.05$  mm (cf. Fig. 1). Three grooves were situated parallel to the central axis of the stylet, at  $120^\circ$  intervals. Three fibers (noted  $F_1$ ,  $F_2$ , and  $F_3$ ) were embedded inside the grooves such that  $F_1$ ,  $F_2$ , and  $F_3$  were at the same distance from the central axis of the stylet. Each fiber  $F_i$  ( $i \in [1,3]$ ) had nine FBGs (noted  $\text{FBG}_1^{(i)}, \dots, \text{FBG}_9^{(i)}$ ). Those FBGs were separated by intervals of 20 mm along the stylet's length such that,  $\forall k \in [1, \dots, 9]$ ,  $\text{FBG}_k^{(1)}$ ,  $\text{FBG}_k^{(2)}$ , and  $\text{FBG}_k^{(3)}$  had the same longitudinal position along the stylet. By measuring the wavelength of the light reflected by the FBGs, the 3D curvature and temperature along the stylet can be determined. Knowing the 3D curvature, it is possible to reconstruct the stylet deflection (and consequently the needle deflection when the stylet is inserted inside the needle) at regularly sampled position (every 1 mm). The procedure to reconstruct the 3D needle deflection by measuring the reflected FBG wavelengths was described by Roesthuis *et al.* and Park *et al.*<sup>20,21</sup>

To determine the amplitude of the reflected wavelength, a measurement device for FBG sensors was used (*FBG-scan 804D*, *FBGS*, *Geel*, *Belgium*). This device is composed of broadband LED source to light the optical fibers, a spectrum analyzer (monochromator) to measure the reflected wave-

length, and a fast optical switch which alternatively routes the three optical fibers to the LED source and spectrum analyzer. A computer controls the device and automatically determines the stylet's deflection using a LabVIEW program. This program could also determine the update rate and latency of the needle deflection measurement, which were dependent on the switching speed, the light integration time of the monochromator, and the needle deflection computation time.

With this system, we can monitor the deflection of the needle. To derive the position of the whole needle, the position and orientation of the stylet at one or more stylet points need to be determined. This can be done using a MR-based calibration, as follows.

## 2.B. MR-based calibration of the FBG-based measurement

In the scope of this study, an experimental protocol is proposed in order to assess the FBG-based needle tracking procedure under MR-imaging. In this setup, the base of the stylet is fixed in space (for example with a clamp) such that this point cannot move or rotate. A MR-based calibration is then performed prior to the measurements of the needle position in order to determine the position and orientation of the stylet at the fixation point (called the "reference point" in the scope of this study). Once the calibration is done, the tracking of the needle can be performed without having to subsequently reapply the calibration. This section describes this MR-based calibration.

If we assume that no image distortion occurred during the MR-imaging, the axes  $X_{MR}$ ,  $Y_{MR}$ , and  $Z_{MR}$  of the MR image are coincident with the axes  $X$ ,  $Y$ , and  $Z$  of the physical spatial coordinate system. A way to determine the position and orientation of the stylet at the reference point is to register this point to the  $X_{MR}$ ,  $Y_{MR}$ , and  $Z_{MR}$ -coordinate system. To achieve this, we propose the following procedure:

1. Several (at least 2) different needle shapes are measured with FBG-based sensing during simultaneous MR imaging. For that, we can insert the stylet into two needles (with different shapes) introduced beforehand into a phantom.
2. The MR-based needle shapes stem from a segmentation step.
3. A rigid registration of the MR and the FBG-based measurements of the needle shapes is then performed. The rigid registration of the MR and FBG-based measurement consists of determining six parameters: three parameters of translations along  $X_{MR}$ ,  $Y_{MR}$ , and  $Z_{MR}$  (noted  $t_x$ ,  $t_y$ , and  $t_z$ ) and three angles of rotation about  $X_{MR}$ ,  $Y_{MR}$ , and  $Z_{MR}$  (noted  $\theta_x$ ,  $\theta_y$ , and  $\theta_z$ ). To find those parameters, paired points between the MR and the FBG-based measurements at regular sample positions along the needle are determined. A gradient driven optimization is then performed to find the values of  $t_x$ ,  $t_y$ ,  $t_z$ ,  $\theta_x$ ,  $\theta_y$ , and  $\theta_z$ . This gradient driven optimization consists of minimizing the distances between those paired points after transformation (translations and rotations). The method to perform this rigid registration is detailed in the Appendix.
4. Once MR and FBG-based measurements are registered, the determination of the stylet position and orientation at the reference point in the  $X_{MR}$ ,  $Y_{MR}$ , and  $Z_{MR}$ -coordinate system is straightforward.

The proposed method involves an immobilization of the stylet base and therefore may be limiting in a clinical workflow. This issue will be discussed in Sec. 4.

## 2.C. Experimental evaluation of FBG-based sensing for real-time needle tracking during MR-guided intervention

This section presents three experiments which aim as follows:

- To assess the accuracy and MR-compatibility of the FBG-based sensing system (cf. Sec. 2.C.1).
- To evaluate the accuracy, precision, update rate, and latency of the complete tracking device under MR imaging using the MR-based calibration presented in Sec. 2.B (cf. Sec. 2.C.2).

In the following experiments, the 3D MR images were acquired with a 1.5 T MR-scanner using a 3D spectral presaturation with inversion recovery (SPIR) sequence ( $TR = 2.9$  ms,  $TE = 1.44$  ms, voxel size =  $1.2 \times 1.45 \times 1$  mm<sup>3</sup>, and number of signal average = 2). This sequence was chosen because it is commonly used to reconstruct a needle, in practice, of HDR brachytherapy at the University Medical Center Utrecht (Netherlands) (UMCU). The employed field of view was approximately  $60 \times 250 \times 250$  mm<sup>3</sup> in order to image the whole length of the needle. The scan time to cover the whole volume was 5 min and 37 s.

### 2.C.1. Accuracy and MR compatibility of FBG-based sensing

To evaluate the accuracy and MR-compatibility of the FBG-based tracking system, we performed the two following experiments:

First, to evaluate the accuracy during MR-imaging, a needle (titanium needle  $1.9 \times 200$  mm from *Elekta, Veenendaal, The Netherlands*) was placed inside the MR scanner bore and its shape was imposed by a specially designed plastic mold with different known 2D paths (cf. Fig. 2). For paths 1, 2, and 3, the deflection of the needle was measured by FBG-based sensing during MR-imaging along four orientations (i.e.,  $0^\circ$ ,  $90^\circ$ ,  $180^\circ$ ,  $270^\circ$ ), by rotating the needle along its longitudinal axis [cf. Fig. 3(a)]. The error between the FBG-based measurement and the gold standard shape was then calculated.

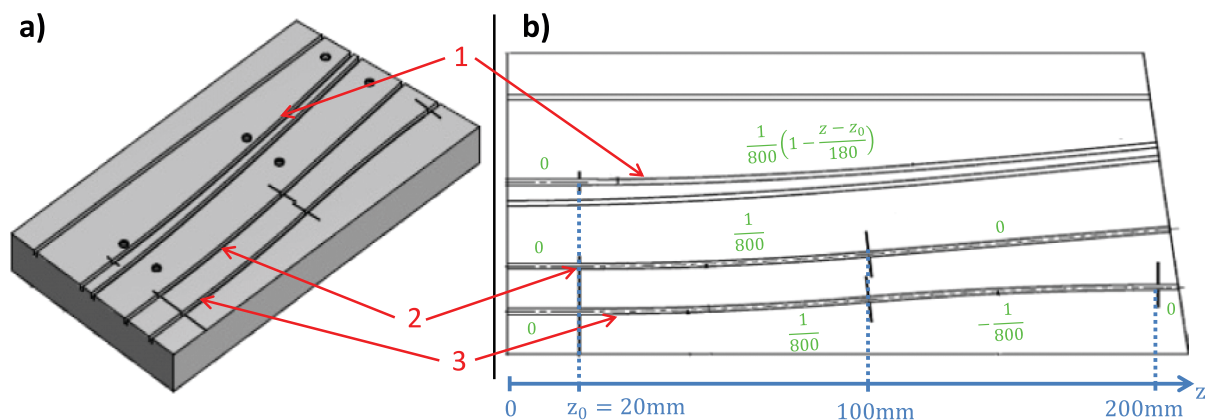


FIG. 2. (a) presents the schematic in 3D of the mold used. The three paths used for the experiment are noted as 1, 2, and 3. (b) is a schematic of the upper view of the mold. The curvatures (in mm<sup>-1</sup>) of the paths 1, 2, and 3 are depicted in green. (See color online version.)

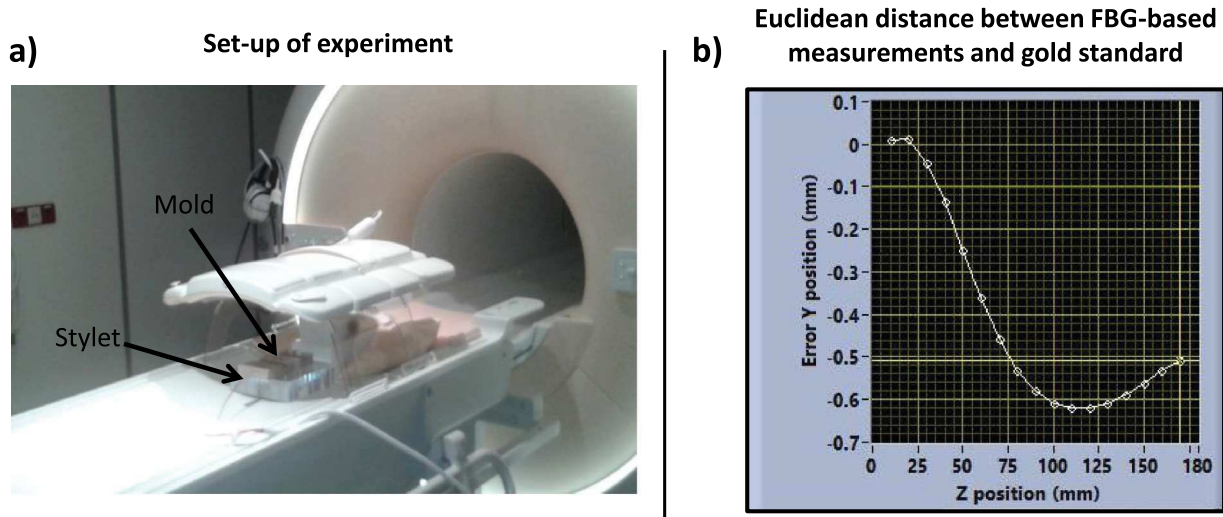


FIG. 3. (a) is a picture of the experimental setup for the gold standard test using the mold inside the MR scanner bore (the setup was shifted out of scanner for photograph). (b) presents the typical example of the Euclidean distance between a known shape and the FBG-based measurement.

Second, to evaluate the impact of FBG-based sensing measurement on MR-imaging, four plastic ProGuide 6F Sharp needles (*Elekta, Veenendaal, The Netherlands*) with a length of 195 mm were introduced in an agar phantom. The corresponding needle shapes were measured with FBG-based sensing during simultaneous MR imaging [cf.

Figs. 4(a) and 4(b)]. The MR-based needle shapes stem from a manual segmentation step. A rigid registration of the obtained MR- and the FBG-based needle measurement was then performed using the algorithm described in the Appendix. After registration, the error between the FBG and MR-based needle position measurements was assessed:

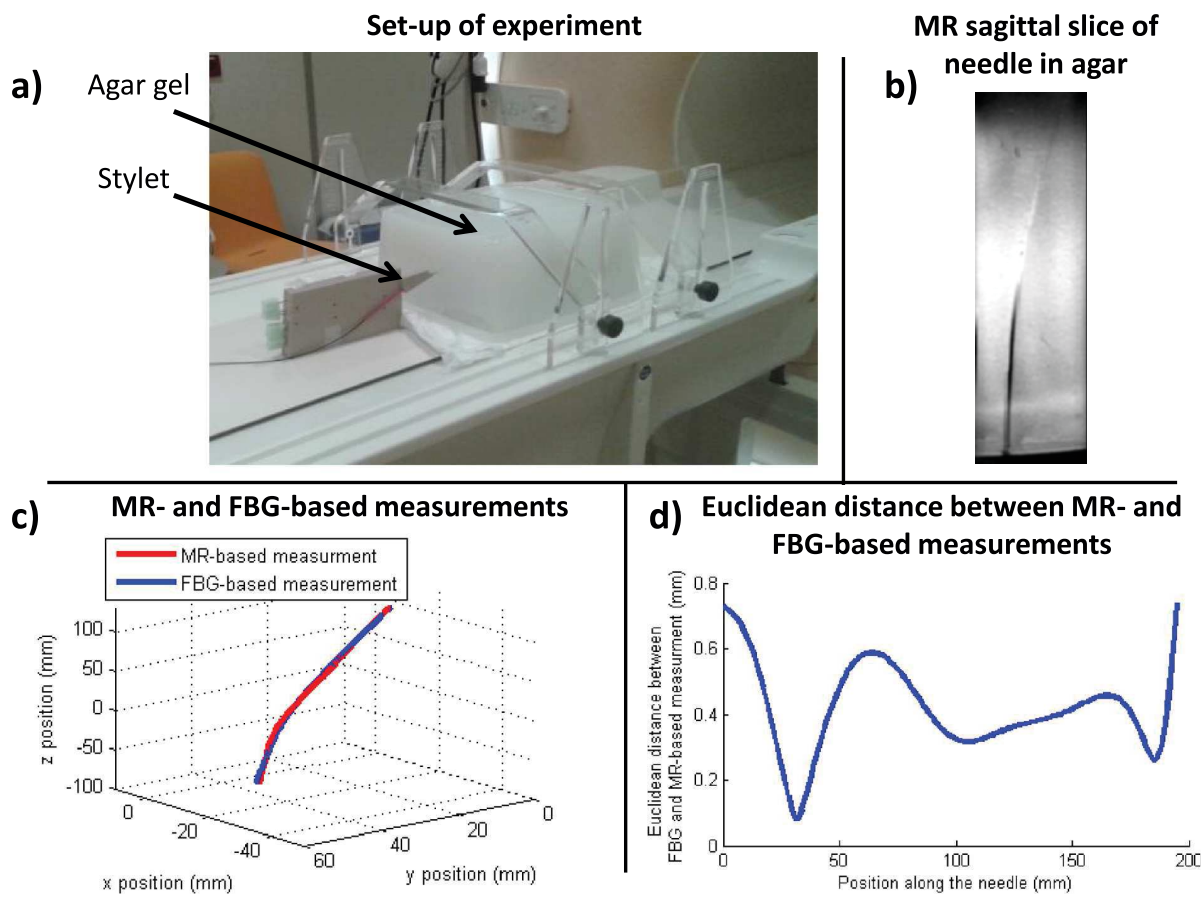


FIG. 4. (a) presents a picture of the experimental setup consisting of evaluating the impact of FBG-based sensing measurement on MR-imaging (the setup was shifted out of scanner for photograph). (b) shows the MR image of one needle, (c) represents the MR and the FBG-based measurement after rigid registration, and (d) represents the Euclidean distance between the MR- and FBG-based measurements along the needle.

For this purpose, the Euclidean distances between the paired points (see Subsection 1 of the Appendix) were calculated.

### 2.C.2. Assessment of the proposed FBG-based needle tracking system

The following experiment was performed to assess the complete needle tracking procedure using the calibration protocol described in Sec. 2.B:

*Step 1.* A flexible needle of 93 mm (ProGuide 6F Sharp by Elekta, Veenendaal, The Netherlands) was placed into a prostate phantom (CIRS, Model 053-I, Ultrasound Prostate Training Phantom).

*Step 2.* The plastic holder of the FBG-based sensing device [cf. Fig. 1(a)] was fastened to a support fixed on the MR table [cf. Fig. 5(a)]. That way, the stylet base was fixed in space with no possibility of translation or rotation.

*Step 3.* The needle shape was measured with FBG-based sensing during simultaneous MR imaging in five different configurations: the phantom was moved for each configuration by approximately one centimeter, along the left–right

axis. That way the needle position was different in each configuration.

*Step 4.* Two of those configurations were used to perform the MR-based calibration and determine the position and orientation of the stylet base (see Sec. 2.B).

*Step 5.* The three other configurations were used to assess the complete FBG-based tracking system: the FBG and MR-based needle position measurements were compared. For this purpose, paired MR and FBG-based points were determined at regular interval (1 mm) along the needle using the algorithm described in Subsection 1 of the Appendix and their corresponding Euclidean distances were calculated.

To assess the repeatability of the results, steps 4 and 5 were repeated for all possible pairs of configurations.

## 3. RESULTS

### 3.A. Accuracy and MR compatibility evaluation of the FBG-based sensing

This section presents the results of the experiments which aim to assess the accuracy and MR-compatibility of the FBG-

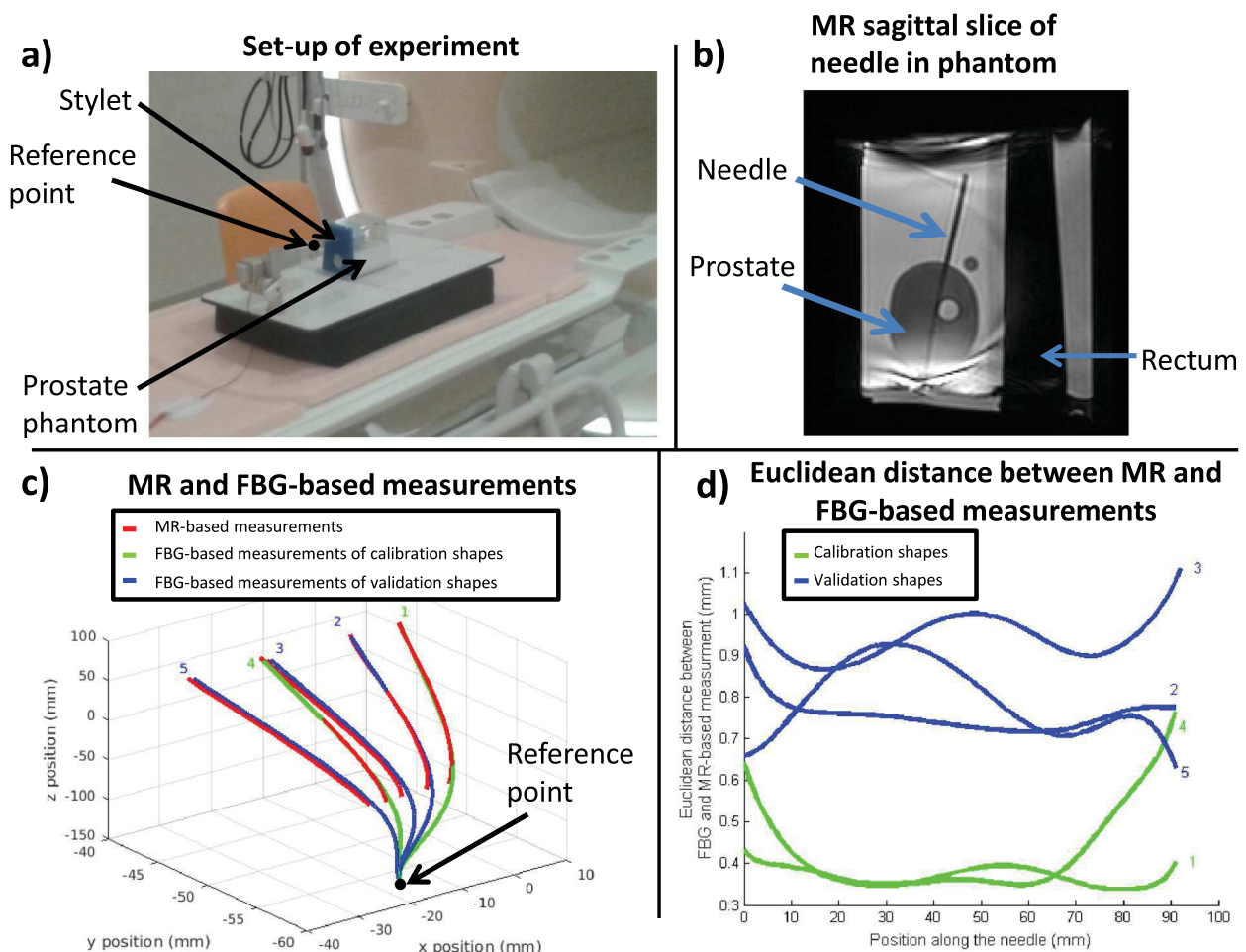


FIG. 5. (a) presents the setup of the experiment consisting of assessing the FBG-based needle tracking system (the setup was shifted out of scanner for photograph). (b) is a MR sagittal slice of the phantom with the inserted needle. (c) represents the MR and the FBG-based measurement after rigid registration. The two configurations used for the calibration of the reference point are in green, the configurations to validate the protocol are in blue. (d) represents the Euclidean distance between the MR and FBG-based tracking measurement along the needle. (See color online version.)

based tracking system (the experimental method is described in Sec. 2.C.1). For all tested needle shapes, the average difference between the FBG-based measurement and the gold standard values (known shapes given by the mold) was 0.27 mm. A characteristic example (path 1 of the mold) is presented in Fig. 3(b): the average(minimum, maximum) absolute difference between the FBG-based measurement and the known shape was 0.42 mm(0.01, 0.62 mm). For the second experiment with four needles in agar phantom, the mean Euclidean distance between MR and FBG-based paired points along the needle was 0.42 mm on average over the four tested needles. A typical example is presented in Figs. 4(c) and 4(d): the average(minimum, maximum) Euclidean distance between MR and FBG-based paired points along the needle was 0.42 mm(0.08, 0.74 mm).

### 3.B. Assessment of the proposed FBG-based needle tracking system

This section presents the results of the experiment which consists of validating the complete needle tracking system. The experimental method is described in Sec. 2.C.2. Over all tested scenarios, the average(standard deviation) Euclidean distance between MR and FBG-based paired points along the needle was 0.79 mm(0.37 mm). In particular, for the paired points at the tip of the needle, the average(standard deviation) Euclidean distance was 1.10 mm(0.45 mm). The update rate and the latency of the needle position measurement were around 100 ms and 300 ms, respectively. The latency and update rate include the integration time of the light received by the monochromator (90 ms) and the computation time of the needle deflection (order of magnitude of a few milliseconds). A typical example is presented in Figs. 5(c) and 5(d): the average(minimum, maximum) Euclidean distance between MR and FBG-based needle position measurements along the needle configurations 2, 3, and 5 (which corresponds to the configurations used to assess the needle tracking system) was 0.76 mm(0.72, 0.93 mm), 0.94 mm(0.87, 1.11 mm), and 0.79 mm(0.63, 0.93 mm), respectively. The average(minimum, maximum) Euclidean distance of the needle tip measurements was 0.84 mm(0.63, 1.11 mm). The largest deviations between the FBG and MR-based measurements were situated close to the outer borders of the phantom.

## 4. DISCUSSION

This paper presents a FBG-based sensing device which is able to track and reconstruct a needle (including catheter or tube) during a medical procedure. This device can track a needle deflection with a high accuracy (0.27 mm on average) in an MR environment. In addition, this report shows that the average Euclidean distance between MR and FBG-based measurements of the needle position after registration was comparable to the uncertainty of MR-based measurements (corresponding to the uncertainty of the manual segmentation) estimated at half the voxel size in the MR image. This indicates that the FBG-based sensing device is not significantly

influenced by the MR environment. Finally, the FBG-based needle tracking device can measure the needle position with an accuracy of 0.79 mm and a precision (standard deviation) of 0.37 mm on average in comparison to the MR-based measurement. In particular, the accuracy and precision of the needle tip is 1.10 and 0.45 mm, respectively. Moreover, the update rate of the needle position measurement is 100 ms and its latency 300 ms.

The inaccuracy related to MR-based measurement can have two origins: inaccuracy in the manual needle segmentation and distortion of the MR-images. Regarding the inaccuracy in the manual needle segmentation, the error was estimated to half the voxel size of the MR images (voxel size =  $1.2 \times 1.45 \times 1 \text{ mm}^3$ ). Regarding the distortion of the MR-image, a quality assessment of the MR was performed prior to the measurements using an ACR phantom with a length of 148 mm and a diameter of 190 mm. Based on this quality assessment, the maximum error found at the border of the ACR phantom was less than 1 mm. Since all MR-images of the experiments presented in this paper were within 100 mm from the MR isocenter, negligible errors are expected to be related to MR-image distortion. The accuracy of the MR-based measurement was therefore estimated to half the voxel size of the MR images.

Since the FBG-based sensing stylet is composed of MR-compatible materials, this device is eligible to be used in a MR environment. Another method eligible in a MR environment is described by Wang *et al.*<sup>18</sup> In this study, a real-time active MR tracking method has been proposed. Multiple microcoils are integrated into metallic stylets. These stylets are used to insert the needles into the tissue. The catheter trajectory is reconstructed by pulling out the stylet from the catheter while the microcoils are tracked using a dedicated MR sequence. In comparison to this active MR tracking method, the accuracy of FBG-based sensing is higher (1.5 mm on average with the active MR tracking method vs 0.8 mm on average with FBG-based tracking). Also the update rate of the FBG-based needle tracking is higher and latency is lower (around 10 s acquisition time per catheter with the MR tracking method vs 100 ms update rate and 300 ms latency with FBG-based sensing). Besides, de Oliveira *et al.*<sup>17</sup> proposed a needle tracking method using MR in the case of endorectal biopsy device. This tracking method has also a lower update rate and higher latency (the total duration of the tracking sequence is about 10 min).

Finally, although MRI presents a lot of advantage such as high contrasts of soft tissues which is useful for organs/tumor delineation, FBG-based needle tracking can also *a priori* be done under a different imaging modality such as ultrasound, computed tomography, or x-ray. In that scenario, other needle tracking methods (which are not MR-compatible) have been recently developed. Kaya *et al.*<sup>22</sup> proposed a method to determine automatically the tip of a needle using 2D ultrasound imaging: the needle tip is estimated with the Gabor filter-based image processing algorithm, and the estimation noise is reduced with the Kalman filter. In that study, the tip location was measured and compared with optical tracking system. The Euclidean distance of the tip position was found to be

1.17 mm. Additionally, a 3D electromagnetic needle tracking system was recently developed:<sup>23–26</sup> a stylet, composed of miniature sensor coils, is immersed in alternating magnetic fields. The resulting electric signal of the sensor coils is then converted to detect the position of the stylet (and therefore the needle when the stylet is inserted in the needle's lumen). The tracking accuracy experiments showed that positional errors were higher (typically 1 mm) compared with FBG-based needle tracking. In addition, the accuracy was dependent on disturbing equipment around.

The benefit of MRI was twofold in the scope of our study: (1) it allowed determining the position and the orientation of the base and (2) it provided a gold standard of the needle shape. This allowed reaching the following endpoints of our paper: (1) to demonstrate the potential of FBG-based needle tracking for the determination of the needle position with high frame rate and low latency and (2) to demonstrate the potential of the latter under on-line MRI. Regarding the determination the position and the orientation of the stylet base, we proposed a simple protocol involving the fixation of the stylet base and the determination of its position and orientation using a MR-based calibration. In the proposed MR calibration, several (at least 2) needle shapes [see (1) in Sec. 2.B] are used to determine the stylet position and orientation at the reference point. This way, the determination of the stylet's position and orientation at the reference point is more accurate: if only one needle shape is used for the registration, the determination of the orientation about the longitudinal axis of the stylet may not be accurate (especially if the needle shape is straight).

A limitation of the proposed tracking protocol arises from the fact that our system is now implemented with the stylet in a fixed support. Although this condition was fulfilled in our experiments, this may not be the case under clinical practice. In a clinical workflow, to know the position and orientation of the stylet base, it should be mounted in a flexible and tracked support that is fixed to the table. This special support could be a robot that supports the insertion of the needle such as those currently developed in several institutes.<sup>27</sup> In particular, at our institution (the UMCU), a MR-compatible single needle robotic device which is fixed to the MR couch is currently under development.<sup>28</sup> Knowing the needle mounting position of the robot in the MR coordinate space means that we can determine the complete shape of the needle in the MR coordinate system. In our view, the current promising results provide justification to continue investing in further improvements of the clinical implementation of the FBG tracking technology within an MR-guided workflow.

Furthermore, the clinical benefits of such a system would be twofold:

1. For real-time tracking of needle during insertion. The fast and accurate feedback of the needle position will help the steering of the needle and warn the user in case of deviations from the planned needle track: better dose coverage and less toxicity would then be expected due to less needle positioning errors.

2. For fast and automatic reconstruction of the needle after insertion. The authors expect that with FBG tracking, less time will be spent compared to manual segmentation of a needle with possibly a better accuracy. This would allow a shorter overall procedure time and enable update of the dose plan with feedback on the needle positioning error.

Future works will involve preclinical and clinical evaluations of the setup.

## 5. CONCLUSION

The proposed FBG-based needle tracking method is able to determine the position of the whole needle with an accuracy of 0.79 mm, a precision (standard deviation) of 0.37 mm, an update rate of 100 ms, and a latency of 300 ms. The proposed approach is a good candidate for the measurement and the compensation of needle positioning errors during the procedure. This would allow an improved needle guidance and reconstruction. Moreover, the dose plan may be updated accordingly using a suited feedback strategy based on the residual needle deviations.

## ACKNOWLEDGMENTS

The authors thank the European Research Council (Project No. ERC-2010-AdG-20100317, Sound Pharma) and the ITEA (Project No. 12026, SoRTS).

## CONFLICT OF INTEREST DISCLOSURE

This study was funded by Philips Medical Systems Nederland B.V. M. Borot de Battisti is funded by Philips Medical Systems Nederland B.V., M. Moerland is a principal investigator on a contract funded by Philips Medical Systems Nederland B.V., and G. Hautvast and D. Binnekamp are full-time employees of Philips Medical Systems Nederland B.V.

## APPENDIX: OPTIMIZATION STRATEGY TO PERFORM THE RIGID REGISTRATION OF THE MR AND FBG-BASED NEEDLE POSITION MEASUREMENT

This section details the method employed to find the transformation between the FBG and the segmented MR-based measurement of a needle. Six transformation parameters are determined: three parameters of translations, noted  $t_x$ ,  $t_y$ , and  $t_z$ , along  $X_{MR}$ ,  $Y_{MR}$ , and  $Z_{MR}$  (the axis of the MR image) and three angles of rotation, noted  $\theta_x$ ,  $\theta_y$ , and  $\theta_z$ , about  $X_{MR}$ ,  $Y_{MR}$ , and  $Z_{MR}$ . A way to determine the value of  $t_x$ ,  $t_y$ ,  $t_z$ ,  $\theta_x$ ,  $\theta_y$ , and  $\theta_z$  is as follows: first, to determine paired MR and FBG-based measurement points at regular intervals along the needle and then to minimize the distance between the paired MR and FBG-based measurement points after transformation.

## 1. Determination of the paired MR and FBG-based measurement points at regular intervals along the needle

It is noticeable that the FBG-based measurement gives the needle's shape at regularly sampled position (every 1 mm) along the stylet. Consequently, to determine the corresponding MR points, the MR based needle shape needs to be analytically modeled: a 3D parametric polynomial fitting of the MR-based points is chosen with the following general form:

$$\begin{cases} x(t) = a_n t^n + a_{n-1} t^{n-1} + \dots + a_0 \\ y(t) = b_n t^n + b_{n-1} t^{n-1} + \dots + b_0 \\ z(t) = t \end{cases} \quad (A1)$$

The polynomial order  $n$  is optimized exhaustively by following two conditions: (1) the order must be as small as possible to avoid over-fitting and (2) the maximum fitting error must be lower than the typical uncertainties of the manually segmented points (estimated at half the voxel size in the MR image).

With this model, the corresponding points of the MR-based measurement can easily be determined by sampling the model at same positions along the stylet compared to the FBG-based measurement points.

## 2. Determination of the transformations parameters

The next step is to determine the value of  $t_x, t_y, t_z, \theta_x, \theta_y,$  and  $\theta_z$  using a minimization of the distance between the MR and FBG-based paired points after transformation (rotations and translations). For this purpose, we employed a gradient driven optimization method.

Let  $n$  be the total number of paired points, and for all  $i \in [1; n]$ ,  $(x_i^{\text{MR}}, y_i^{\text{MR}}, z_i^{\text{MR}})$  and  $(x_i^{\text{FBG}}, y_i^{\text{FBG}}, z_i^{\text{FBG}})$  are their corresponding coordinates of the MR and FBG-based measurement points. To minimize the distance between the paired points, the following cost function  $C(t_x, t_y, t_z, \theta_x, \theta_y, \theta_z)$  [corresponding to the squared average distance between the paired points after transformation (rotations and translations)] is minimized:

$$C(t_x, t_y, t_z, \theta_x, \theta_y, \theta_z) = \|P^{\text{MR}} - A_{\text{FBG} \rightarrow \text{MR}}(t_x, t_y, t_z, \theta_x, \theta_y, \theta_z) P^{\text{FBG}}\|_2^2, \quad (A2)$$

where  $P^{\text{MR}}$  and  $P^{\text{FBG}}$  are the MR and FBG-based measurement point matrices,

$$P^{\text{MR}} = \begin{pmatrix} x_1^{\text{MR}} & \dots & x_n^{\text{MR}} \\ y_1^{\text{MR}} & \dots & y_n^{\text{MR}} \\ z_1^{\text{MR}} & \dots & z_n^{\text{MR}} \\ 1 & \dots & 1 \end{pmatrix}, P^{\text{FBG}} = \begin{pmatrix} x_1^{\text{FBG}} & \dots & x_n^{\text{FBG}} \\ y_1^{\text{FBG}} & \dots & y_n^{\text{FBG}} \\ z_1^{\text{FBG}} & \dots & z_n^{\text{FBG}} \\ 1 & \dots & 1 \end{pmatrix}, \quad (A3)$$

and  $A_{\text{FBG} \rightarrow \text{MR}}(t_x, t_y, t_z, \theta_x, \theta_y, \theta_z)$  is the transformation matrix,

$$A_{\text{FBG} \rightarrow \text{MR}}(t_x, t_y, t_z, \theta_x, \theta_y, \theta_z) = T_x(t_x) T_y(t_y) T_z(t_z) R_x(\theta_x) R_y(\theta_y) R_z(\theta_z), \quad (A4)$$

where  $T_x(t_x)$ ,  $T_y(t_y)$ , and  $T_z(t_z)$  are the matrices of translation along the  $X_{\text{MR}}$ ,  $Y_{\text{MR}}$ , and  $Z_{\text{MR}}$  axis and  $R_x(\theta_x)$ ,  $R_y(\theta_y)$ , and

$R_z(\theta_z)$  are the matrices of rotation about the  $X_{\text{MR}}$ ,  $Y_{\text{MR}}$ , and  $Z_{\text{MR}}$  axis.

Since  $A_{\text{FBG} \rightarrow \text{MR}}(t_x, t_y, t_z, \theta_x, \theta_y, \theta_z)$  is not linear along  $\theta_x, \theta_y,$  and  $\theta_z$ , the minimization of  $C(t_x, t_y, t_z, \theta_x, \theta_y, \theta_z)$  is therefore performed using a gradient driven method.

<sup>a)</sup>Electronic mail: M.E.P.Borot@umcutrecht.nl

<sup>1</sup>J. Venselaar, A. S. Meigooni, D. Baltas, and P. J. Hoskin, *Comprehensive Brachytherapy: Physical and Clinical Aspects* (Taylor & Francis, Washington, 2012).

<sup>2</sup>M. Borot de Battisti, M. Maenhout, B. Denis de Senneville, G. Hautvast, D. Binnekamp, J. J. W. Lagendijk, M. van Vulpen, and M. A. Moerland, "An automated optimization tool for high-dose-rate (HDR) prostate brachytherapy with divergent needle pattern," *Phys. Med. Biol.* **60**, 7567–7583 (2015).

<sup>3</sup>B. L. Gorissen, D. den Hertog, and A. L. Hoffmann, "Mixed integer programming improves comprehensibility and plan quality in inverse optimization of prostate HDR brachytherapy," *Phys. Med. Biol.* **58**, 1041–1057 (2013).

<sup>4</sup>Å. Holm, Å. Carlsson Tedgren, and T. Larsson, "Heuristics for integrated optimization of catheter positioning and dwell time distribution in prostate HDR brachytherapy," *Ann. Oper. Res.* **236**, 319–339 (2013).

<sup>5</sup>G. Strassmann, P. Olbert, A. Hegele, D. Richter, E. Fokas, N. Timmesfeld, R. Hofmann, and R. Engenhart-Cabillic, "Advantage of robotic needle placement on a prostate model in HDR brachytherapy," *Strahlenther. Onkol.* **187**, 367–372 (2011).

<sup>6</sup>M. Cengiz, S. Gurdalli, U. Sele, F. Yildiz, Y. Saglam, E. Özyar, and I. L. Atahan, "Effect of bladder distension on dose distribution of intracavitary brachytherapy for cervical cancer: Three-dimensional computed tomography plan evaluation," *Int. J. Radiat. Oncol., Biol., Phys.* **70**, 464–468 (2008).

<sup>7</sup>J. Hung, S. Shen, J. F. D. L. Santos, and R. Y. Kim, "Image-based 3D treatment planning for vaginal cylinder brachytherapy: Dosimetric effects of bladder filling on organs at risk," *Int. J. Radiat. Oncol., Biol., Phys.* **83**, 980–985 (2012).

<sup>8</sup>P. J. Hoskin, P. J. Bownes, P. Ostler, K. Walker, and L. Bryant, "High dose rate afterloading brachytherapy for prostate cancer: Catheter and gland movement between fractions," *Radiother. Oncol.* **68**, 285–288 (2003).

<sup>9</sup>N. N. Stone, J. Roy, S. Hong, Y.-C. Lo, and R. G. Stock, "Prostate gland motion and deformation caused by needle placement during brachytherapy," *Brachytherapy* **1**, 154–160 (2002).

<sup>10</sup>V. Lagerburg, M. A. Moerland, M. van Vulpen, and J. J. Lagendijk, "A new robotic needle insertion method to minimise attendant prostate motion," *Radiother. Oncol.* **80**, 73–77 (2006).

<sup>11</sup>C. Kirisits, M. J. Rivard, D. Baltas, F. Ballester, M. D. Brabandere, R. van der Laarse, Y. Niatsetski, P. Papagiannis, T. P. Hellebust, J. Perez-Calatayud, K. Tanderup, J. L. Venselaar, and F.-A. Siebert, "Review of clinical brachytherapy uncertainties: Analysis guidelines of GEC-ESTRO and the AAPM," *Radiother. Oncol.* **110**, 199–212 (2014).

<sup>12</sup>M. Borot de Battisti, B. Denis de Senneville, M. Maenhout, G. Hautvast, D. Binnekamp, J. J. W. Lagendijk, M. van Vulpen, and M. A. Moerland, "Adaptive planning strategy for high dose rate prostate brachytherapy—A simulation study on needle positioning errors," *Phys. Med. Biol.* **61**, 2177–2195 (2016).

<sup>13</sup>R. Pötter, "Image-guided brachytherapy sets benchmarks in advanced radiotherapy," *Radiother. Oncol.* **91**, 141–146 (2009).

<sup>14</sup>G. Groenendaal, M. R. Moman, J. G. Korporaal, P. J. van Diest, M. van Vulpen, M. E. Philippens, and U. A. van der Heide, "Validation of functional imaging with pathology for tumor delineation in the prostate," *Radiother. Oncol.* **94**, 145–150 (2010).

<sup>15</sup>J. C. Dimopoulos, P. Petrow, K. Tanderup, P. Petric, D. Berger, C. Kirisits, E. M. Pedersen, E. van Limbergen, C. Haie-Meder, and R. Pötter, "Recommendations from gynaecological (GYN) GEC-ESTRO working group (IV): Basic principles and parameters for MR imaging within the frame of image based adaptive cervix cancer brachytherapy," *Radiother. Oncol.* **103**, 113–122 (2012).

<sup>16</sup>A. L. Damato and A. N. Viswanathan, "Magnetic resonance-guided gynecologic brachytherapy," *Magn. Reson. Imaging Clin. North Am.* **23**, 633–642 (2015).

<sup>17</sup>A. de Oliveira, J. Rauschenberg, D. Beyersdorff, W. Semmler, and M. Bock, "Automatic passive tracking of an endorectal prostate biopsy device using phase-only cross-correlation," *Magn. Reson. Med.* **59**, 1043–1050 (2008).

- <sup>18</sup>W. Wang, A. N. Viswanathan, A. L. Damato, Y. Chen, Z. Tse, L. Pan, J. Tokuda, R. T. Seethamraju, C. L. Dumoulin, E. J. Schmidt, and R. A. Cormack, "Evaluation of an active magnetic resonance tracking system for interstitial brachytherapy," *Med. Phys.* **42**, 7114–7121 (2015).
- <sup>19</sup>K. R. Henken, J. Dankelman, J. J. van den Dobbelsteen, L. K. Cheng, and M. S. van der Heiden, "Error analysis of FBG-based shape sensors for medical needle tracking," *IEEE/ASME Trans. Mechatronics* **19**, 1523–1531 (2014).
- <sup>20</sup>Y. L. Park, S. Elayaperumal, B. Daniel, S. C. Ryu, M. Shin, J. Savall, R. J. Black, B. Moslehi, and M. R. Cutkosky, "Real-time estimation of 3-D needle shape and deflection for MRI-guided interventions," *IEEE/ASME Trans. Mechatronics* **15**, 906–915 (2010).
- <sup>21</sup>R. J. Roesthuis, M. Kemp, J. J. van den Dobbelsteen, and S. Misra, "Three-dimensional needle shape reconstruction using an array of fiber bragg grating sensors," *IEEE/ASME Trans. Mechatronics* **19**, 1115–1126 (2014).
- <sup>22</sup>M. Kaya, E. Senel, A. Ahmad, O. Orhan, and O. Bebek, "Real-time needle tip localization in 2D ultrasound images for robotic biopsies," in *International Conference on Advanced Robotics (ICAR)* (IEEE, Istanbul, Turkey, 2015), pp. 47–52.
- <sup>23</sup>S. Boutaleb, E. Racine, O. Fillion, A. Bonillas, G. Hautvast, D. Binnekamp, and L. Beaulieu, "Performance and suitability assessment of a real-time 3D electromagnetic needle tracking system for interstitial brachytherapy," *J. Contemp. Brachytherapy* **7**, 280–289 (2015).
- <sup>24</sup>E. Poulin, E. Racine, D. Binnekamp, and L. Beaulieu, "Fast, automatic, and accurate catheter reconstruction in HDR brachytherapy using an electromagnetic 3D tracking system," *Med. Phys.* **42**, 1227–1232 (2015).
- <sup>25</sup>J. Zhou, E. Sebastian, V. Mangona, and D. Yan, "Real-time catheter tracking for high-dose-rate prostate brachytherapy using an electromagnetic 3D-guidance device: A preliminary performance study," *Med. Phys.* **40**, 021716 (7pp.) (2013).
- <sup>26</sup>A. L. Damato, A. N. Viswanathan, S. M. Don, J. L. Hansen, and R. A. Cormack, "A system to use electromagnetic tracking for the quality assurance of brachytherapy catheter digitization," *Med. Phys.* **41**, 101702 (7pp.) (2014).
- <sup>27</sup>T. K. Podder, L. Beaulieu, B. Caldwell, R. A. Cormack, J. B. Crass, A. P. Dicker, A. Fenster, G. Fichtinger, M. A. Meltsner, M. A. Moerland, R. Nath, M. J. Rivard, T. Salcudean, D. Y. Song, B. R. Thomadsen, and Y. Yu, "AAPM and GEC-ESTRO guidelines for image-guided robotic brachytherapy: Report of Task Group 192," *Med. Phys.* **41**, 101501 (27pp.) (2014).
- <sup>28</sup>M. R. Van den Bosch, M. R. Moman, M. van Vulpen, J. J. Batterman, E. Duiveman, L. J. van Schelven, H. de Leeuw, J. J. W. Lagendijk, and M. A. Moerland, "MRI-guided robotic system for transperineal prostate interventions: Proof of principle," *Phys. Med. Biol.* **55**, 133–140 (2010).